richments of 13% (Fig. 1) and may actually result in a slight depletion. Consequently, reactions 5a and 5b must be responsible for the enrichment. A tunable diode laser experiment (*19*) revealed that the symmetric molecule formed in reaction 5b may contribute only 10% to the enrichment, and therefore reaction 5a must carry a large rate coefficient advantage of ~43% to account for the mass spectrometric observations.

More detailed conclusions from the relative rate coefficients that are shown in Table 1 can only be drawn when the values of the three homonuclear reaction rates for ozone are known. Using the absolute values for $^{16}O + {}^{32}O_2$ and $^{18}O + {}^{36}O_2$ that were derived by Anderson *et al.* (*20*), we inferred by interpolation that the rate coefficient for $^{17}O + {}^{34}O_2$ is 6.15×10^{-34} cm^6 s^{-1} (*21*). The missing rates contributing to a specific isotope can now be calculated from the total enrichments measured in scrambled oxygen mixtures (Fig. 1). The derived rate coefficient ratios in Table 2 represent the sum of the symmetric and asymmetric reaction channels, which may be separated in future tunable diode laser experiments. The rule derived for atomic oxygen collisions also holds for reactions with heteronuclear species: ^{16}O collisions result in a higher rate of formation, whereas collisions with ^{18}O are close to the formation rate of the reaction $^{16}O + {}^{32}O_2$. Reaction $^{16}O + {}^{18}O^{16}O$ is the fastest, $^{16}O + {}^{17}O^{16}O$ and $^{17}O + {}^{18}O^{17}O$ are similar but slower, $^{17}O + {}^{16}O^{17}O$ and $^{18}O + {}^{17}O^{18}O$ are even slower, and $^{18}O + {}^{16}O^{18}O$ is the slowest.

The results presented here provide new insights into the puzzling ozone isotope effect. It is not the symmetry of a molecule that determines the magnitude of the enrichment, but rather it is the nature of the collision process that occurs when ozone is produced in a nitrogen-oxygen gas mixture.

References and Notes

1. D. Krankowsky and K. Mauersberger, *Science* **274**, 1324 (1996).
2. D. Krankowsky *et al.*, *Geophys. Res. Lett.* **22**, 1713 (1995); J. C. Johnston and M. H. Thiemens, *J. Geophys. Res.* **102**, 25395 (1997).
3. A summary of stratospheric $^{50}O_3$ enrichments results can be found in work by F. W. Irion *et al.*, *Geophys. Res. Lett.* **23**, 2377 (1996).
4. M. H. Thiemens and T. Jackson, *ibid.* **15**, 639 (1988); *ibid.* **17**, 717 (1990); J. Morton, J. Barnes, B. Schueler, K. Mauersberger, *J. Geophys. Res.* **95**, 901 (1990).
5. Y. L. Yung *et al.*, *J. Geophys. Res.* **102**, 10857 (1997).
6. The isotope composition of atmospheric oxygen is $[^{16}O] = 99.756\%$, $[^{17}O] = 0.038\%$, and $[^{18}O] = 0.205\%$ throughout the troposphere and stratosphere.
7. The enrichments listed in percent are calculated with the expression $E(\%) = [({}^{M}O_3/{}^{48}O_3)_{\mathrm{meas}}/({}^{M}O_3/{}^{48}O_3)_{\mathrm{calc}} - 1] \times 100\%$ with mass $M = 49$ through 54. For ozone produced in atmospheric oxygen, we used the values listed in (6) to calculate the statistical ratios.
8. J. E. Heidenreich III and M. H. Thiemens, *J. Chem. Phys.* **84**, 2129 (1986).
9. S. M. Anderson *et al.*, *ACS Symp. Ser.* **502**, 155 (1992).
10. S. M. Anderson and K. Mauersberger, *J. Geophys. Res.* **100**, 3033 (1995); D. W. Arnold, C. Xu, E. H. Kim, D. M. Neumark, *J. Chem. Phys.* **101**, 912 (1994).
11. G. I. Gellene, *Science* **274**, 1344 (1996).
12. J. J. Valentini, *J. Chem. Phys.* **86**, 6757 (1987); D. R. Bates, *Geophys. Res. Lett.* **15**, 13 (1988); W. L. Morgan and D. R. Bates, *Planet. Space Sci.* **40**, 1573 (1992); K. S. Griffith and G. I. Gellene, *J. Chem. Phys.* **96**, 4403 (1992).
13. S. M. Anderson, D. Hülsebusch, K. Mauersberger, *J. Chem. Phys.* **107**, 5385 (1997).
14. K. Mauersberger, J. Morton. B. Schueler, J. Stehr, S. M. Anderson, *Geophys. Res. Lett.* **20**, 1031, 1993.
15. N. W. Larsen, T. Pedersen, J. Sehested, *Int. J. Chem. Kinet.* **23**, 331 (1991).
16. J. Sehested, O. J. Nielsen, H. Egsgaard, *J. Geophys. Res.* **100**, 20979 (1995); *ibid.* **103**, 3545 (1998).
17. J. A. Kaye and D. F. Strobel, *ibid.* **88**, 8447 (1983).
18. K. Mauersberger, *Rev. Sci. Instrum.* **48**, 1169 (1977).
19. S. M. Anderson, J. Morton, K. Mauersberger, *Chem. Phys. Lett.* **156**, 175 (1989).
20. The actual values found by Anderson *et al.* (*13*) are $^{16}O + {}^{32}O_2 + M = 6.05 \times 10^{-34}$ cm^6 s^{-1}, $^{18}O + {}^{36}O_2 + M = 6.25 \times 10^{-34}$ cm^6 s^{-1}, $^{18}O + {}^{32}O_2 + M = 6.26 \times 10^{-34}$ cm^6 s^{-1}, and $^{16}O + {}^{36}O_2 + M = 8.98 \times 10^{-34}$ cm^6 s^{-1}. A ratio for the isotope exchange reaction rates $k_{^{18}O}/k_{^{16}O} = 1.245$ was used; this ratio is in agreement with the experimental data presented in (*13*) and in Fig. 1.
21. The purity of the available ^{17}O gas was not sufficiently high to obtain an absolute rate coefficient that was comparable in accuracy to $^{16}O + {}^{32}O$ and $^{18}O + {}^{36}O$.
22. We thank S. M. Anderson at Augsburg College, who contributed substantially to the experiment and obtained the first set of rate coefficients.

14 September 1998; accepted 1 December 1998

Self-Assembly of Ordered Microporous Materials from Rod-Coil Block Copolymers

Samson A. Jenekhe* and X. Linda Chen

Rod-coil diblock copolymers in a selective solvent for the coil-like polymer self-organize into hollow spherical micelles having diameters of a few micrometers. Long-range, close-packed self-ordering of the micelles produced highly iridescent periodic microporous materials. Solution-cast micellar films consisted of multilayers of hexagonally ordered arrays of spherical holes whose diameter, periodicity, and wall thickness depended on copolymer molecular weight and composition. Addition of fullerenes into the copolymer solutions also regulated the microstructure and optical properties of the microporous films. These results demonstrate the potential of hierarchical self-assembly of macromolecular components for engineering complex two- and three-dimensional periodic and functional mesostructures.

Ordered mesoporous solids with nanoscale pore sizes are of interest in areas such as catalysis, sensors, size- and shape-selective separation media, adsorbents, and scaffolds for composite materials synthesis (*1*, *2*). Those with pore sizes on the order of 50 nm to 10 μm are also of interest for applications in photonics, optoelectronics, lightweight structural materials, and thermal insulation (*2*–*5*). Most current general methods for preparing diverse porous materials use self-organized surfactants, block copolymers, or colloidal particles as templates in conjunction with sol-gel techniques (*1*–*3*). In these methods, the organic templates are eventually removed by thermal decomposition or solvent extraction to achieve the porous solid. Recently reported hollow spherical micelles of rod-coil diblock copolymers (*6*) represent a previously unknown class of colloidal particles (*7*). Their self-organization into long-range crystalline order could open the way to novel colloidal crystals (*8*, *9*), unusual microgels, and direct self-assembly of ordered microporous materials.

Polymer latex and silica spheres are known to form colloidal crystals (*8*, *9*), but long-range ordering of suspensions of block copolymer micelles into body-centered cubic (bcc) and face-centered cubic (fcc) lattices was observed and elucidated more recently (*10*). Micelles of coil-coil block copolymers in a selective solvent for one of the blocks are spheres consisting of a dense core of the insoluble block and a diffuse corona of the solvated block (*10*–*12*). Copolymer architecture and solution chemistry have been used to vary their diameter between about 10 and 80 nm and the corona thickness relative to the core radius (*10*–*12*). Micellar crystallization into either an fcc or a bcc lattice is determined by the length scale and steepness of repulsive interactions that can be controlled by the ratio of the coronal layer thickness to the core radius (*10*). However, the implications of the unusual micellar structures of rod-coil block copolymers (*6*, *13*) for regulating these repulsive interactions, micellar crystallization, and crystal lattice selection are yet to be investigated.

We report the self-organization of hollow

Departments of Chemical Engineering and Chemistry, University of Rochester, Rochester, NY 14627–0166, USA.

*To whom correspondence should be addressed. E-mail: jenekhe@che.rochester.edu

spherical micelles from a rod-coil diblock copolymer system in a selective solvent for the flexible-coil block and their long-range, close-packed self-ordering into iridescent, ordered microporous solids. This hierarchical self-assembly approach to microporous solids represents a nontemplate strategy (Fig. 1). The micellar structure, consisting of a hollow core, a rodlike inner shell, and a flexible-coil outer corona, has a diffuse corona characteristic of coil-coil block copolymer micelles (*10*, *12*). Steric repulsion-driven self-ordering and crystallization of coil-coil diblock micelles and their demonstrated control through the corona block length (*10*) are thus also viable options here. The rod-coil diblock copolymer system we investigated is poly(phenylquinoline)-*block*-polystyrene (PPQ_mPS_n, where *m* and *n* are the number of repeat units of the respective blocks) in carbon disulfide (CS_2), which is a selective solvent for PS block. The specific diblock compositions we studied are $PPQ_{10}PS_{300}$, $PPQ_{10}PS_{1000}$, and $PPQ_{50}PS_{2000}$, which are either identical to those we previously reported (*6*, *13*) or similarly made. The basic synthetic chemistry is that associated with the rigid, rodlike conjugated PPQ homopolymer (*14*), which is highly fluorescent and has nonlinear optical properties (*15*).

We investigated solutions (0.005 to 1.0 weight % diblock) in CS_2 and monolayer and multilayer films cast from them at room temperature (25°C). Direct optical, fluorescence, and scanning electron microscopy observations of discrete micellar aggregates and their higher order assembly into large-scale periodic microstructures were made. The possible effects of both the local structure of the micellar building block and the large-scale periodic microstructure on the spontaneous emission of the PPQ chromophores of the diblocks were probed by previously described steady-state and time-resolved photoluminescence techniques (*16*).

Theoretical studies of the possible equilibrium structures of micelles of rod-coil block copolymers in a selective solvent for the coil-like block have been reported (*17*). Because of the difficulty of efficient space-filling packing of rodlike blocks into a spherical or a cylindrical core, various alternative space-filling core-corona models, such as disklike cylindrical micelles and monolayer and bilayer "hockey puck" micelles, have been proposed (*17*). However, experimental data have heretofore been unavailable to test these models (*18*). Our experimental results show that rod-coil diblock chains solve the steric problem associated with packing rodlike blocks radially into a sphere in a surprising way not anticipated by theory: a hollow sphere. Fluorescence photomicrographs of micelles formed by $PPQ_{10}PS_{300}$ in CS_2 provide evidence of hollow spheres (Fig. 2, A and B). The shape of the discrete micellar aggregates looks somewhat like red blood cells because of distortion and partial collapse of the hollow spheres due to drying. Additional microscopic observations under bright field and crossed polarizers confirmed that the micelles formed by all three copolymer samples had approximate diameters of 3 to 5 μm. Polarized optical microscopy indicated that the micelles were highly ordered. This ordering originates from orientationally ordered radial packing of the rigid, rodlike blocks; micellar aggregates of coil-coil block copolymers lack such order (*11*–*12*). The hollow spherical structure of these rod-coil diblock micelles in CS_2 is, however, different from that formed by the same copolymers in trifluoroacetic acid/dichloromethane (a selective solvent for the rodlike blocks) (*6*, *13*) in that here the solvated coil-like blocks are on the convex side. A profound consequence of the stiffness asymmetry of a rod-coil diblock copolymer is thus that the same macromolecule in two different selective solvents can self-organize into two qualitatively different colloidal particles: hollow hard spheres and hollow soft spheres.

Self-ordering of these hollow soft spheres into two- (2D) and three-dimensional (3D) periodic structures was studied by optical and electron microscopy of micellar films cast from diblock solutions of varying initial concentrations in ways similar to previous studies of colloidal crystallization of polymer latex spheres (*8*, *9*). Only discrete, nonaggregated micelles were obtained from very dilute solutions between 0.005 and 0.01 weight % (Fig. 2, A and B). However, even at 0.01 weight %, the particle number density is sufficiently high for the onset of 2D micellar ordering to be visible in regions of a monolayer film (Fig. 2B, arrows). Micellar films cast from 0.5 weight % had a controllable thickness of about 4.5 to 35 μm and consisted of stacks of one to eight layers of hexagonally close-packed (hcp) 2D lattices of spherical air holes in a polymeric matrix. An example is the ~27-μm-thick micellar film of $PPQ_{10}PS_{300}$, which reveals a 2D hcp structure when viewed from the top (Fig. 2C) and was visually highly iridescent at various reflection angles, akin to a credit card hologram. The air holes revealed by carefully peeling off part of the top layer with an adhesive tape largely reflect the original hollow spherical micelles. The moderate mechanical properties of these self-ordered micellar films

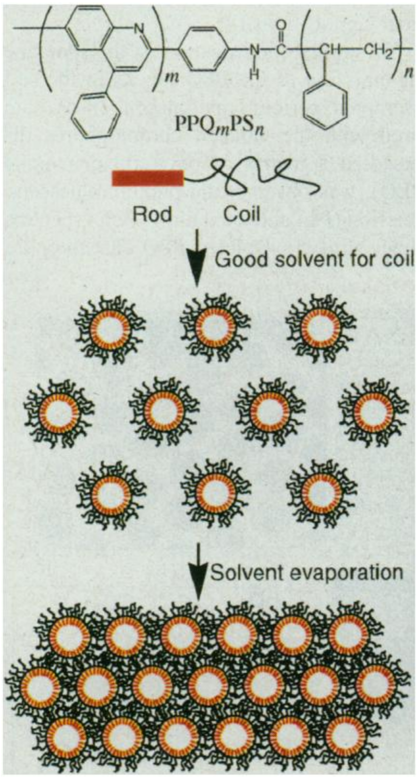

Fig. 1. Molecular structure of the rod-coil diblock copolymer PPQ_mPS_n and schematic illustration of its hierarchical self-assembly into ordered microporous materials.

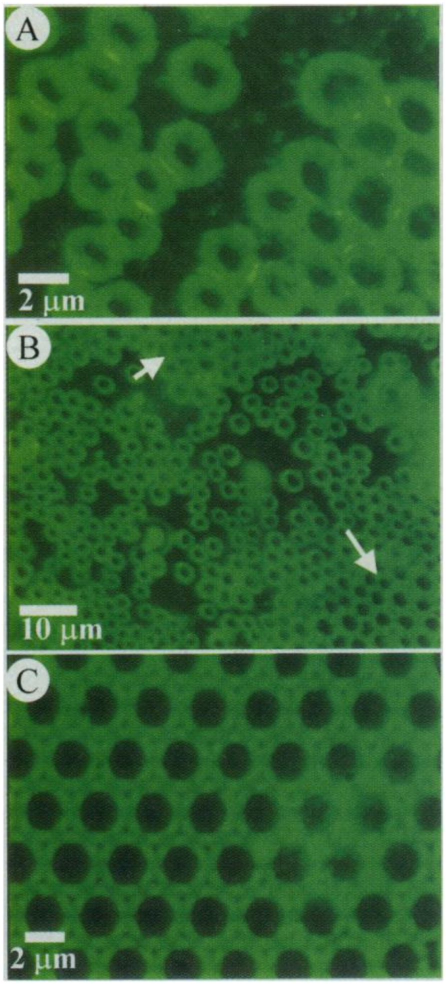

Fig. 2. Fluorescence photomicrographs of solution-cast micellar films of $PPQ_{10}PS_{300}$ obtained by ambient air drying of different diblock solution concentrations in CS_2: (**A**) 0.005 weight %, (**B**) 0.01 weight %, and (**C**) 0.5 weight %. Arrows in (B) indicate regions of self-ordering.

suggest that substantial interdigitation of the polystyrene coronal chains occurs between the micellar building blocks of the microporous solid.

Defect-free microstructure of the periodic microporous films of all three block copolymers covered areas as large as 1 cm^2 and varied with composition and molecular weight. From the polarized optical and scanning electron micrographs of micellar films of $PPQ_{50}PS_{2000}$ (Fig. 3, A to C), a 2D hcp lattice of spherical air holes having a diameter (D) of 3.4 ± 0.2 μm and a center-to-center hole periodicity (p) of 4.4 ± 0.2 μm was observed from the top layer. The ~31-μm film consisted of seven layers of air hole lattices of which the top layer is open (Fig. 3, B and C). The progressive decreases of the hole diameter and periodicity of the microstructure with the PS block length were approximately linear (Fig. 3D), decreasing to 2.6 ± 0.2 and 2.8 ± 0.2 μm, respectively, for micellar films of $PPQ_{10}PS_{300}$. The minimum wall thickness h ($= p - D$), which was in the range of 0.2 to 1.0 μm for the three copolymer compositions, also varied linearly with the PS coronal chain length. Evidence of the 3D order of these multilayer films includes their colorful iridescence (*2*, *8*, *9*) and observation of ordered arrays of the air holes when multilayer films were viewed from the side or by sequential removal of layers from the top (*19*).

Addition of small amounts (<20 mg of fullerene per gram of diblock) of fullerene (C_{70} or C_{60}) into the solutions in CS_2 substantially modified the microstructural parameters of the ordered microporous films (Fig. 4). Although these fullerene-containing micellar films had superior iridescence colors compared with similar microporous films without fullerene, they were more brittle, with visible cracks. The hole diameter and periodicity decreased with the amount of fullerene loading, up to 29 and 25% reductions, respectively, at 10 mg of C_{70} per gram of $PPQ_{10}PS_{300}$ (Fig. 4B). The wall thickness increased slightly with fullerene loading. Similar effects of fullerene C_{70} or C_{60} on self-organized microporous films of $PPQ_{10}PS_{1000}$ and $PPQ_{50}PS_{2000}$ were observed. Self-assembly of microporous films was no longer observed in any of the three diblock copolymers at high fullerene loading (>20 mg/g). These results suggest that the fullerene is incorporated within the PS corona of the micellar building blocks, as expected from their mutual compatibility (*6*). These findings also suggest a simple way of controlling the functional properties of the microporous materials independently of copolymer architecture and composition.

Because of their spatially periodic variation of refractive index, these self-organized ordered microporous materials with or without fullerenes are promising, easy to produce photonic band gap structures (*2*, *4*). These periodic dielectric composites of air holes (refractive index $n_o = 1$) and diblock walls ($n_o = 1.6$ for PS and 1.8 for PPQ) have a high refractive index contrast. The higher index contrast in fullerene-containing micellar films, C_{70} ($n_o = 1.94$) and C_{60} ($n_o = 2.00$ to 2.12) (*20*), can explain their superior optical properties. However, the present hole diameters and periodicities are comparable to infrared (IR) wavelengths. Reductions in D and p to sizes comparable to visible wavelengths are desirable for some photonic and optoelectronic applications (*4*).

Substantial modification of the spontaneous emission of the PPQ blocks in the self-assembled, periodic microporous films, compared with the isolated chromophores dispersed in a matrix of poly(ethylene oxide) (PEO), was observed by photoluminescence emission (PL) and excitation (PLE) spectroscopies (Fig. 5). Isolated PPQ chromophores of the $PPQ_{10}PS_{300}$ diblock have emission and excitation bands at 466 and 393 nm, respectively. In contrast, the micellar films of

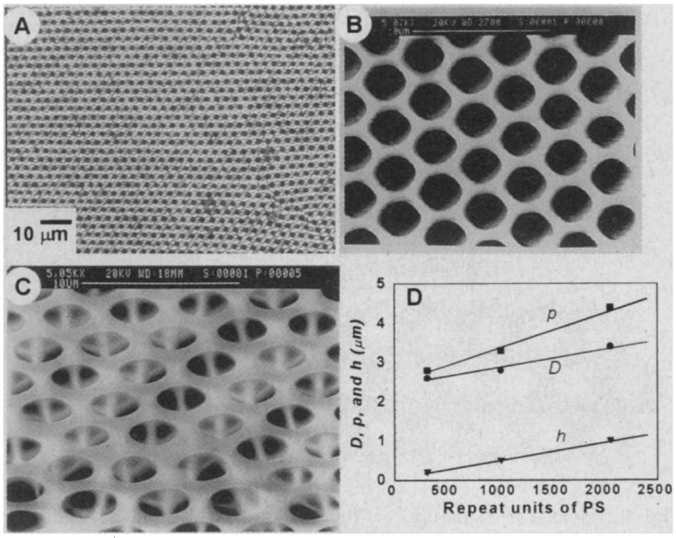

Fig. 3. (**A**) Polarized optical and (**B** and **C**) scanning electron micrographs of microporous micellar films obtained from a 0.5 weight % $PPQ_{50}PS_{2000}$ diblock solution by solution casting on a glass slide (A) and an aluminum substrate [(B) and (C)]. The scanning electron micrograph samples were coated with a 10-nm gold layer. The scanning electron micrograph image in (B) is the top view, and that in (C) is of the same sample tilted 45° from the beam axis to reveal 3D structure. (**D**) Variation of *D*, *p*, and *h* of ordered microporous films with the number of PS repeat units in the diblocks.

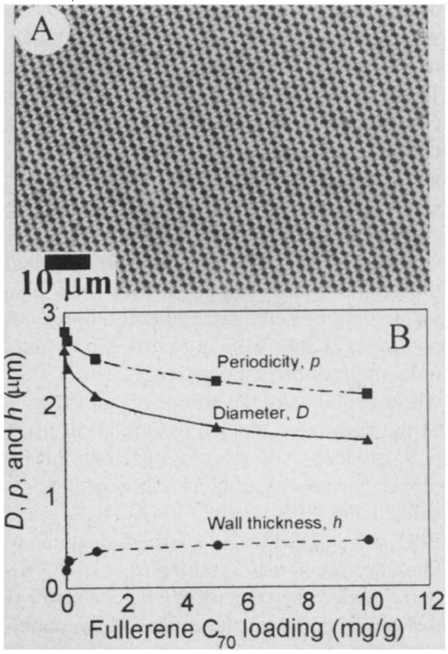

Fig. 4. (**A**) Polarized optical micrograph of a microporous micellar film of $PPQ_{10}PS_{300}$ obtained from a 0.5 weight % solution containing 5 mg of C_{70} per gram of diblock. (**B**) Dependence of microstructural parameters of micellar films of the same diblock on fullerene loading.

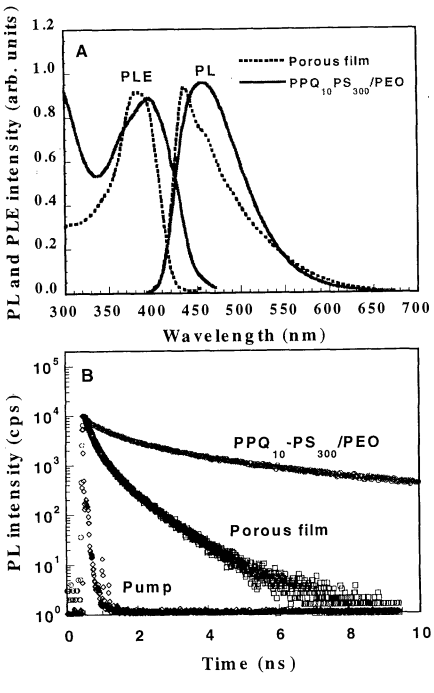

Fig. 5. (**A**) PL emission (390-nm excitation) and PLE excitation (460-nm emission) spectra of a micellar film of $PPQ_{10}PS_{300}$ and of the same diblock chains homogeneously dispersed (0.1 weight %) in a PEO film. (**B**) PL decay dynamics of the same samples in (A) when excited at 360 nm and monitored at 490 nm.

$PPQ_{10}PS_{300}$ cast from a 0.5 weight % solution have blue-shifted PL and PLE spectra with peaks at 437 and 388 nm, respectively (Fig. 5A), and the absorption band observed in the PLE is narrower. Time-resolved PL decay dynamics of the fluorescent PPQ blocks as isolated chains in PEO revealed two lifetimes [1.1 ns (30%) and 4.7 ns (70%)] compared with one lifetime (0.93 ns) (Fig. 5B) in the micellar films. This represents a large reduction in the excited state lifetime of PPQ chromophores in the microporous micellar films. Because the emission band is far removed from photonic band gaps of these microporous films, which are expected to be in the IR region, we rule out the large-scale periodic microstructure as the origin of the observed modification of photophysical properties. The decrease in lifetime is also the opposite of the predicted effect of a photonic crystal on spontaneous emission (*4*). H-Aggregation (*21*) of the PPQ blocks and hence the local structure of the micellar building blocks best explains the observed photophysical properties. H-Aggregation of the rigid rodlike blocks implies that they are orientationally aligned close to the radial direction in the spherical micellar assemblies (Fig. 1). Such an H-aggregation of conjugated molecules can lead to novel cooperative optical and nonlinear optical properties (*21*).

Because the size, mesostructure, and properties of micellar building blocks can be tailored through copolymer architecture and composition as well as the solution chemistry (*10–13*), we suggest that this hierarchical self-assembly approach is quite general for preparing periodic mesoporous polymeric materials. Besides photonic band gap materials and their associated applications (*4*), the ordered micellar films and their self-assembly process may have uses as models in tissue engineering and biomaterials (*22*), fabrication of molecular electronic devices (*23*), optically tunable and responsive coatings, and processing of "soft" colloidal materials. By combining different micellar building blocks and colloidal particles such as dendrimers or polymer lattices, self-assembly of very unusual periodic mesoscopic structures with tailorable functions may be possible.

References and Notes

1. C. T. Kresge, M. E. Leonowics, W. J. Roth, J. C. Vartuli, J. S. Beck, *Nature* **359**, 710 (1992); A. Sayari, *Chem. Mater.* **8**, 1840 (1996); Q. Huo, D. I. Margolese, G. D. Stucky, *ibid.*, p. 1147; D. Zhao *et al.*, *Science* **279**, 548 (1998); E. Krämer, S. Förster, C. Göltner, M. Antionetti, *Langmuir* **14**, 2027 (1998).
2. J. E. G. J. Wijnhoven and W. L. Vos, *Science* **281**, 802 (1998).
3. A. Imhor and D. J. Pine, *Nature* **389**, 948 (1997).
4. E. Yablonovitch, *J. Opt. Soc. Am. B* **10**, 283 (1993); J. D. Joannopoulos, P. R. Villeneuve, S. Fan, *Nature* **386**, 143 (1997); J. Martorell and N. M. Lawandy, *Phys. Rev. Lett.* **65**, 1877 (1990); H. Miguez *et al.*, *Appl. Phys. Lett.* **71**, 1148 (1997).
5. T. Bitzer, *Honeycomb Technology* (Chapman and Hall, London, 1997).
6. S. A. Jenekhe and X. L. Chen, *Science* **279**, 1903 (1998).
7. R. J. Hunter, *Foundations of Colloid Science*, vol. 1 (Clarendon, Oxford, UK, 1987); R. Buscall, T. Corner, J. F. Stagemen, Eds., *Polymer Colloids* (Elsevier, London, 1985); D. F. Evans and H. Wennerström, *The Colloidal Domain: Where Physics, Chemistry, Biology, and Technology Meet* (Wiley-VCH, New York, 1994).
8. A. Kose and S. J. Hachisu, *Colloid Interface Sci.* **46**, 460 (1974); S. Hachisu and S. Yoshimura, *Nature* **283**, 188 (1980); N. A. Clark, A. J. Hurd, B. J. Ackerson, *ibid.* **281**, 57 (1979); P. Pieranski, *Contemp. Phys.* **24**, 25 (1983); P. N. Pusey and W. van Megen, *Nature* **320**, 340 (1986); P. Bartlett, R. H. Ottewill, P. N. Pusey, *Phys. Rev. Lett.* **68**, 3801 (1992).
9. A. van Blaaderen, R. Ruel, P. Wiltzius, *Nature* **385**, 321 (1997); J. M. Weissman, H. B. Sunkara, A. S. Tse, S. A. Asher, *Science* **274**, 959 (1996).
10. G. A. McConnell, A. P. Gast, J. S. Huang, S. D. Smith, *Phys. Rev. Lett.* **71**, 2102 (1993); G. A. McConnell, M. Y. Lin, A. P. Gast, *Macromolecules* **28**, 6754 (1995); G. A. McConnell and A. P. Gast, *ibid.* **30**, 435 (1997); *Phys. Rev. E.* **54**, 5447 (1996).
11. S. E. Webber, P. Munk, Z. Tuzar, Eds., *Solvents and Self-Organization of Polymers* (Kluwer Academic, Dordrecht, 1996); S. E. Webber, *J. Phys. Chem. B* **102**, 2618 (1998); Z. Tuzar and P. Kratochvil, in *Surface and Colloid Science*, vol. 15, E. Matijevic, Ed. (Plenum, New York, 1993); pp. 1–83.
12. A. Halperin, M. Tirrell, T. P. Lodge, *Adv. Polymer Sci.* **100**, 31 (1992); S. Förster and M. Antonietti, *Adv. Mater.* **10**, 195 (1998); L. Zhang and A. Eisenberg, *J. Am. Chem. Soc.* **118**, 3168 (1996); *Science* **268**, 1728 (1995).
13. X. L. Chen and S A Jenekhe, in preparation.
14. A. K. Agrawal and S. A. Jenekhe, *Macromolecules* **26**, 895 (1993); *Chem. Mater.* **8**, 579 (1996).
15. A. K. Agrawal, S. A. Jenekhe, H. Vanherzeele, J. S. Meth, *J. Phys. Chem.* **96**, 2837 (1992); S. A. Jenekhe *et al.*, *Chem. Mater.* **9**, 409 (1997).
16. J. A. Osaheni and S. A. Jenekhe, *J. Am. Chem. Soc.* **117**, 7389 (1995); S. A. Jenekhe and J. A. Osaheni, *Science* **265**, 765 (1994).
17. A. N. Semenov and S. V. Vasilenko, *Sov. Phys.* **63**, 70 (1986); A. N. Semenov, *Mol. Cryst. Liq. Cryst.* **209**, 191 (1991); A. Halperin, *Macromolecules* **23**, 2724 (1990); R. Holyst and M. Schick, *J. Chem. Phys.* **96**, 729 (1992); M. Müller and M. Schick, *Macromolecules* **29**, 8900 (1996); D. R. M. Williams and G. H. Fredrickson, *ibid.* **25**, 3561 (1992); D. R. M. Williams and A. Halperin, *Phys. Rev. Lett.* **71**, 1557 (1993); E. Raphael and G. P. de Gennes, *Physica A* **177**, 294 (1991); *Makromol. Chem. Macromol. Symp.* **62**, 1 (1992).
18. G. Widawski, M. Rawiso, B. Francois, *Nature* **369**, 387 (1994); B. Francois, O. Pitois, J. Francois, *Adv. Mater.* **7**, 1041 (1995). From a small-angle neutron-scattering study of poly(*p*-phenylene)-*block*-polystyrene in a selective solvent for PS, these authors have reported observation of spherical micelles of the conventional dense core-diffuse corona structure with a core diameter of 3 to 5 nm. These rod-coil diblocks and star homopolymers were reported to form ordered microporous films by an unclear phase separation mechanism. Our hierarchical self-assembly model of Fig. 1 can better explain the latter results but is inconsistent with their micellar structure.
19. Distinction between ABCABC- or ABABAB-type stacking of layers and hence whether the 3D lattice was fcc or hcp could not be established.
20. M. S. Dresselhaus, G. Dresselhaus, P. C. Eklund, *Science of Fullerenes and Carbon Nanotubes* (Academic Press, San Diego, CA, 1996).
21. M. Kasha, *Radiat. Res.* **20**, 55 (1963); R. M. Hochstrasser and M. Kasha, *Photochem. Photobiol.* **3**, 317 (1964); V. Czikkely, H. D. Försterling, H. Kuhn, *Chem. Phys.* **6**, 11 (1970); H. Chen, M. S. Farahat, K.-Y. Law, D. G. Whitten, *J. Am. Chem. Soc.* **118**, 2584 (1996).
22. J. H. Fendler, *Membrane Mimetic Chemistry* (Wiley, New York, 1982).
23. F. L. Carter, Ed., *Molecular Electronics II* (Marcel Dekker, New York, 1987).
24. This research was supported by the Office of Naval Research and in part by NSF (grants CTS-9311741 and CHE-9120001) and an Elon Huntington Hooker Fellowship to X.L.C.

30 September 1998; accepted 9 December 1998

Electron Transfer Between Bases in Double Helical DNA

Shana O. Kelley and Jacqueline K. Barton*

Fluorescent analogs of adenine that selectively oxidize guanine were used to investigate photoinduced electron transfer through the DNA π-stack as a function of reactant stacking and energetics. Small variations in these factors led to profound changes in the kinetics and distance dependences of DNA-mediated electron-transfer reactions. Values of β, a parameter reflecting the dependence of electron transfer on distance, ranged from 0.1 to 1.0 per angstrom. Strong stacking interactions result in the fastest electron-transfer kinetics. Electrons are thus transported preferentially through an intrastrand rather than interstrand pathway. Reactant energetics also modulate the distance dependence of DNA-mediated charge transport. These studies may resolve the range of disparate results previously reported, and paradigms must now be developed to describe these properties of the DNA π-stack, which can range from insulator- to "wire"-like.

The base pairs of the DNA double helix, an organized array of aromatic heterocycles, present a novel medium in which to explore π-stack–mediated electron transfer (ET) (*1*). Indeed, base damage and repair in DNA can be promoted across significant distances through long-range ET (*2*). However, experiments addressing ET through DNA using pendant donors and acceptors have provided remarkably different assessments of the electronic coupling provided by DNA (*3–10*).

Beckman Institute, Division of Chemistry and Chemical Engineering, California Institute of Technology, Pasadena, CA 91125, USA. jkbarton@cco.caltech.edu

*To whom correspondence should be addressed.